Digital Discovery

rsc.li/digitaldiscovery

ROYAL SOCIETY
OF CHEMISTRY

PAPER
Matthew D. Witman and Peter Schindler
MatFold: systematic insights into materials discovery
models' performance through standardized cross-validation
protocols

Check for updates

MatFold: systematic insights into materials discovery models' performance through standardized cross-validation protocols†

Matthew D. Witman [ID] *[a] and Peter Schindler [ID] *[b]

Machine learning (ML) models in the materials sciences that are validated by overly simplistic cross-validation (CV) protocols can yield biased performance estimates for downstream modeling or materials screening tasks. This can be particularly counterproductive for applications where the time and cost of failed validation efforts (experimental synthesis, characterization, and testing) are consequential. We propose a set of standardized and increasingly difficult splitting protocols for chemically and structurally motivated CV that can be followed to validate any ML model for materials discovery. Among several benefits, this enables systematic insights into model generalizability, improvability, and uncertainty, provides benchmarks for fair comparison between competing models with access to differing quantities of data, and systematically reduces possible data leakage through increasingly strict splitting protocols. Performing thorough CV investigations across increasingly strict chemical/structural splitting criteria, local *vs.* global property prediction tasks, small *vs.* large datasets, and structure *vs.* compositional model architectures, some common threads are observed; however, several marked differences exist across these exemplars, indicating the need for comprehensive analysis to fully understand each model's generalization accuracy and potential for materials discovery. For this we provide a general-purpose, featurization-agnostic toolkit, MatFold, to automate reproducible construction of these CV splits and encourage further community use in model benchmarking.

Introduction

Understanding and quantifying the generalizability, improvability, and uncertainty of machine learning (ML)-based materials discovery models is critical, especially in applications where downstream experimental validation (synthesis, characterization, and testing) is often time- and cost-intensive. Careful, and sometimes extensive, cross-validation (CV) is required to both avoid erroneous conclusions regarding a model's capabilities and to fully understand its limitations.[1] Withholding randomly selected test data is often insufficient for quantifying a model's performance as this sub-set is drawn from the same distribution that potentially suffers from data leakage. This in-distribution (ID) generalization error is typically minimized during model training and hyperparameter tuning to avoid over/underfitting. Model prediction

uncertainties can be assessed utilizing model ensembling (*e.g.*, for bagged regressor ML models[2,3] and deep neural networks[4,5]) and/or through nested ("double") CV.[6] However, the out-of-distribution (OOD) generalization error constitutes a more useful performance metric for assessing a model's true ability to generalize to unseen data—an especially critical factor when models are used to discover materials with exceptional target properties (*i.e.*, outliers).[7] This error originates from either lack of knowledge (*e.g.*, imbalance in data, or poor data representation) or sub-optimal model architecture and is referred to as being *epistemic*.[4] Evaluating OOD generalization, however, requires more careful considerations during data splitting.

One approach to constructing OOD test sets is to utilize unsupervised clustering with a chosen materials featurization and then conduct leave-one-cluster-out CV (LOCO-CV). For example, on compositional models for superconducting transition temperatures, LOCO-CV revealed how generalizability and expected accuracy are drastically overestimated due to data leakage in random train/test splits.[8] Omee *et al.* have investigated the performance of OOD prediction tasks on MatBench[9] datasets (refractive index, shear modulus, and formation energy) utilizing structure-based graph neural network (GNN) models and LOCO-CV (k-means clustering and t-distributed stochastic neighbor embedding).[10] Hu *et al.* similarly have utilized LOCO-CV to study the improvement of OOD

[a]Sandia National Laboratories, Livermore, California 94551, USA. E-mail: mwitman@sandia.gov

[b]Northeastern University, Boston, Massachusetts 02115, USA. E-mail: p.schindler@northeastern.edu

† Electronic supplementary information (ESI) available: The ΔH_V dataset is provided in the supplementary_files_defects.zip. Additional CV analysis showing inference performance for additional hold-out strategies. MAE heatmaps and parity plots for leave-one-element-out splits. Quartile boxplots of model performance metrics. See DOI: https://doi.org/10.1039/d4dd00250d

generalizability of various domain adaptation algorithms during materials property predictions (experimental band gaps and bulk metallic glass formation ability).[11]

Quantifying distribution shifts in materials databases over time and identifying whether specific samples are OOD have been shown critical for developing databases and models that promote greater robustness and generalizability.[12] To quantify whether data points are OOD can be assessed based on their distance to training data in feature space (*e.g.*, *via* kernel density estimates[2]). Data bias arising from uneven coverage of materials families may also be mitigated by entropy-targeted active learning.[13]

Alternative methods for defining OOD splits without relying on the feature space include using (i) target property ranges, (ii) time or date thresholds when data was added, or (iii) general materials information, such as structure, chemistry, or prototype/class. Splits based on target-property-sorted data[14] can facilitate the discovery of materials with extraordinary target properties[7] and has also been used in "*k*-fold forward CV".[15] Splitting datasets based on when data points were added mimics acquiring new, unseen data that may be realistically considered OOD.[14,16,17] Lastly, the OOD generalization has recently been studied for formation energy models with structural and chemical hold-outs.[18]

To further encourage standardized reporting of these types of detailed insights into generalization performance and limitations of ML-based models in the materials sciences, here we provide "MatFold" as a featurization-agnostic programmatic tool for automatically generating CV splits for arbitrary materials datasets and model architectures, such as structure-based[19] or composition-based[20] models. Specifically, we propose a standardized series of CV splits based on increasingly difficult chemical/structural hold-out criteria, dataset size reduction, nested *vs.* non-nested splits, and others. By assessing model performance across various combinations of MatFold splitting criteria, one could, for example, more fairly compare the performance of differing approaches with the same modeling objectives. This approach allows for a better understanding of how well models' predictions generalize with increasingly difficult chemical or structural hold-out criteria. Additionally, it can determine the expected model improvement with continued data acquisition and assess whether this improvement depends on the splitting criteria used for OOD generalization. Furthermore, the method evaluates whether nested CV ensembles enhance OOD predictions and quantifies the extent of this improvement. It also examines the reliability of uncertainty estimates derived from nested CV ensembles and whether this reliability varies based on the splitting criteria used for assessing generalization.

For practically demonstrating the utility of insights derived from MatFold, we select ML exemplars from our previous work (modeling vacancy formation energies[21] and surface work functions[22]). These are examples in structure-based ML where data leakage can be very problematic since multiple training examples are derived from the same base crystal structure. For example, many structures may contain vacancy sites that are determined to be unique but are in fact nearly identical because

they are only slightly above the symmetry tolerance. Similarly, Miller surfaces from the same base crystal structure may be extremely similar. In either exemplar, the expected model error for inference (*i.e.*, materials screening) can vary by factors of 2–3, depending on the splitting criteria. For comparison we additionally include a standard benchmarking exemplar from MatBench[9] (bulk modulus). Through detailed insights into expected model performance in these exemplars and how it compares/differs across various splitting criteria, dataset sizes, and the exemplars themselves, we motivate MatFold as an easy-to-use, lightweight, and open-source tool for the materials ML community to enable the generation of reproducible data splits that deliver greater insights into model generalizability, improvability, and uncertainty.

MatFold procedure

MatFold serves as a convenient and automated tool to process a user's materials data and systematically generate increasingly difficult CV splits to test a modeling approach's generalizability (Fig. 1). This lightweight, pip-installable Python package requires minimal data preparation and ensures reproducible dataset splits. When generating splits, MatFold creates a JSON file (see ESI Fig. 9†) that allows users to recreate identical splits from the same dataset, at a later time or by different users. This feature makes it easy to share splitting protocols, promoting consistent and reproducible benchmarking. MatFold offers two split methods, $S = \{K$-fold or nested (K, L)-fold$\}$, where K and L are integers chosen by the user. If the user sets K or L to zero then the value is determined by MatFold and is set to be equal to the number of unique split labels (*i.e.*, the created folds are then leave-one-out (LOO)). Outer K-folds can be split on a variety of criteria, $C_K = \{$Random, Structure, Composition, Chemical system = Chemsys, Element, Periodic table (PT) group, PT row, Space group number = SG#, Point group, or Crystal system$\}$, while inner L-folds can be split either randomly or utilizing the same split criteria as the outer splits ($C_L = \{$Random, $C_K\}$). We note that for datasets where each target label corresponds to a unique bulk crystal structure (*e.g.*, Materials Project ID, mpid) the splitting strategies "Random" and "Structure" coincide (which is the case for the $\log(K_{\mathrm{VRH}})$ dataset but not for the ΔH_V and ϕ datasets considered in this work). As shown in Table 1, MatFold provides functionality to artificially reduce the dataset size by a fractional amount D (which applies to the entire dataset before splitting is performed). Furthermore, materials with a specified number of unique chemical elements can be assigned to the training set by default thereby exempting them from the split criteria. This could be, for example, whether the automatic assignment of all binary compounds to the training data is performed, $T = \{$None or Binary$\}$ (the motivation for which is discussed in the next section). For the case where $T =$ Binary and the outer splitting criteria holds out the element Fe, for example, then binary materials like FeO or FeAl would still be included in the training set, even though they would otherwise be placed in the test set under the hold-out criteria. Split labels which make up a small or large fraction of the entire dataset can also be excluded from the test set by specifying
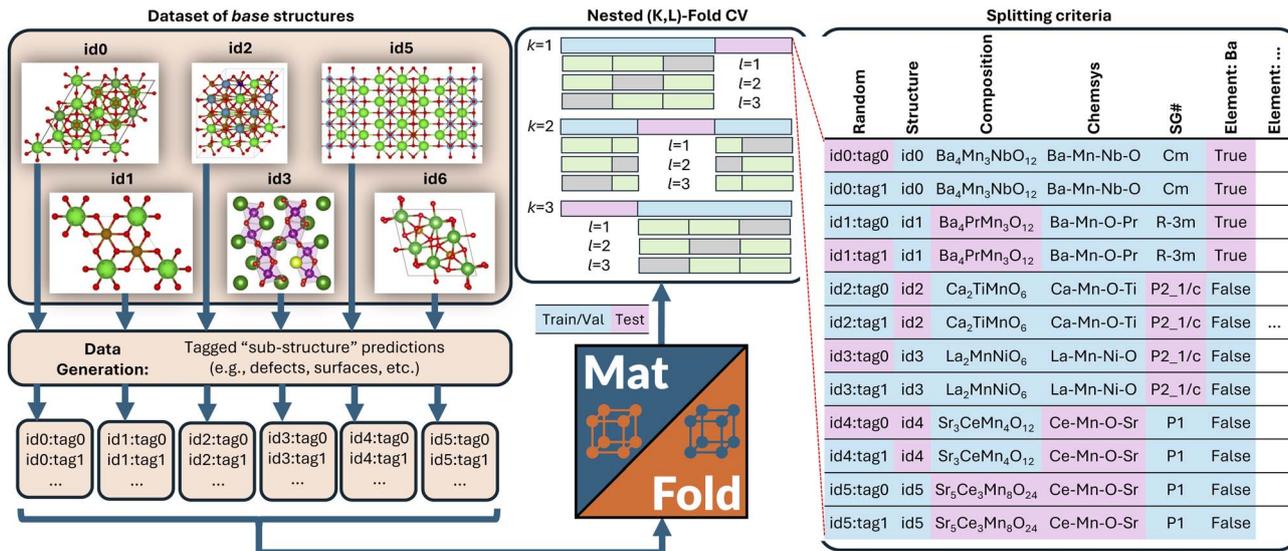
Fig. 1 MatFold processes a set of base crystal structures, each of which may have multiple unique target values per structure (*i.e.*, defect formation energies for unique symmetry sites, work functions for unique Miller surfaces, *etc.*). Nested (K, L)-fold CV train/test splits are automatically generated according to a variety of splitting criteria.

lower or upper limits within MatFold, respectively. This can be utilized to avoid skewed test sets.

Based on the user's choices of D, T, K, L, and C_K, MatFold can typically create thousands of splits. The feasibility of training this many models may depend on the dataset size and modeling approach and may be less feasible, for example, in the training of recently developed universal ML potentials.[23–26] However, dataset and model sizes are often small enough for more specialized ML-based materials discovery models to perform splits across at least some subset of the criteria summarized in Table 1. Subsequent exemplars based on our previous work (modeling vacancy defect formation energies[21] and surface work functions[22]) and a standard MatBench example (modeling bulk modulus[9]), we are able to train thousands of model splits generated by MatFold to obtain improved insights into our models' generalizability and limitations. An overview of the ΔH_V, ϕ, and $\log(K_{VRH})$ datasets and the chosen MatFold split protocols for each are listed in Table 2. Model hyperparameters are fixed at the optimal conditions as determined in the respective previous work.[9,21,22]

To evaluate the model performances, we denote the mean absolute error of an outer test set $MAE = 1/N_k \sum_i |\hat{p}_i - p_i|$, where N_k is the number of samples in the outer fold k, $\hat{p}_i$ is the model prediction of sample i, and p_i the truth value. The expected model performance is given as the ensemble average over the set of all K folds, $\langle\{MAE\}_K\rangle$. For non-nested CV, *i.e.*, K-fold, $\hat{p}_i$ in the kth test set is predicted by a single model trained on the kth train set. For nested CV, *i.e.*, (K, L)-fold, the final prediction is the ensemble average over the set of inner model predictions on the outer test set, $\langle\{\hat{p}_i\}_L\rangle$. The deviation of that ensemble average prediction from the true value is referred to as residuals, calculated as $|p_i - \langle\{\hat{p}_i\}_L\rangle|$. Importantly, nested CV also yields an uncertainty metric *via* the standard deviation over the set of inner model predictions on the outer test set, $\sigma(\{\hat{p}_i\}_L)$.

We note that for datasets with strong imbalances in splitting labels (*e.g.*, an element present in almost the entire dataset *vs.* another element being present only in a tiny fraction of the dataset) the MAE and its standard deviation may be affected by the random seed during split generation. This can be mitigated in MatFold by specifying a minimum and maximum threshold of split label prevalence that determines whether that label is considered during the CV procedure or is always enforced to be in the training set. For example, if oxygen is present in 90% of structures in the dataset and the user specifies a maximum

Table 1 Description of available options and criteria for creating splits with MatFold. PT and LOO stand for periodic table and leave-one-out, respectively

Options	Abbr.	Possibilities
Data fraction	D	$\mathbb{R} \in (0, 1]$
Default train assignment	T	{None, Elemental, Binary, Ternary, …}
Split method	S	{K-fold, (K, L)-fold} $K, L \in \mathbb{N}^+$ (fixed or LOO)
Criteria (outer)	C_K	{Random, Structure, Composition, Chemical System, Element, PT Group, PT Row, Space Group, Point Group, Crystal System}
Criteria (inner)	C_L	{Random, C_K}

Table 2 Overview of the three datasets considered in this work and description of the utilized splitting strategies implemented with MatFold for each

	Vacancy formation energy (ΔH_V)	Work function (ϕ)	Bulk modulus log(K_{VRH})
# Data points	1670	58 332	10 574
# Of unique:			
Structures	250	3716	10 574
Compositions	230	3623	9321
Chemsys	114	2832	6946
Space groups	35	62	173
Elements	18	77	78
$\langle$target$\rangle$	5.8 eV	3.92 eV	1.88 log(GPa)
σ(target)	3.5 eV	0.86 eV	0.37 log(GPa)
Model type	dGNN	RF	{CGCNN,RF}
D	{0.1, 0.25, 0.5, 0.75, 1.0}	{0.05, 0.1, 0.25, 0.5, 1.0}	1.0
T	{None, binary}	None	None
S	{K, (K, L)}	{K, (K, L)}	(K, L)
C_K			
Random	$K = 10, L = 10$	$K = 10, L = 10$	—
Structure	$K = 10, L = 10$	$K = 10, L = 10$	$K = 5, L = 5$
Composition	$K = 10, L = 10$	$K = 10, L = 10$	—
Chemsys	$K = 10, L = 10$	$K = 10, L = 10$	—
Elements	$K = \text{LOO}, L = 10$	$K = \text{LOO}, L = \text{LOO}$	$K = \{\text{LOO}, 5\}, L = 5$
PT group	—	$K = \text{LOO}, L = \text{LOO}$	—
Space group	$K = 10, L = 10$	$K = 10, L = 10$	$K = 5, L = 5$
Point group	—	$K = \text{LOO}, L = \text{LOO}$	—
Crystal Sys	—	$K = \text{LOO}, L = \text{LOO}$	—
C_L	Random	C_K	Random
# Total splits	7480	4046	930

threshold of 0.9, then oxygen-containing structures will be part of the training set by default during CV.

Vacancy formation energy exemplar

Recently we developed a defect GNN (dGNN) modeling approach to directly predict relaxed vacancy formation energies, ΔH_V, from their respective bulk crystal structures.[21] The accompanying open-source dataset[27] specifically computes neutral cation and oxygen vacancies in ∼200 compounds, to which we added the neutral oxygen vacancy formation energies for ∼50 more structures from the work by Wexler et al.[28] in this study (self-consistency between these two datasets was previously determined[21]). Now, we use MatFold to generate ∼7480 possible splits and train/test our model performance, as summarized in Fig. 2 and 4, to better understand the modeling approach's generalizability, improvability, and uncertainty.

Fig. 2a shows density parity plots of all outer test set predictions for C_K = {Random, Structure, Composition, Chemsys, SG#, Elements} and $D = 1.0$, $T = $ None, and S=K-fold, while Fig. 2b shows the same but for $T = $ Binary and S=(K, L)-fold. The color code is on a logarithmic scale with respect to the number of predictions at that grid point. Note that for this dataset, we are able to compute all ΔH_V for at least one of each binary oxide in the

chemical space of interest, motivating the investigation of automatically assigning binaries to the training data. Immediately noticeable in Fig. 2b is the mitigation of over-fitting for some of the largest outliers observed in Fig. 2a. Additional analysis in the ESI,† applicable only to this exemplar, investigates the $C_K = $ Elements parity plots at a more granular level and further reveals insights into the generalization capabilities of dGNN.

Fig. 2c further quantifies the dependence of the expected model error as a function of T, S, and C_K and highlights key conclusions. The expected MAE is strongly influenced by the splitting criteria and generally increases with Random < Structure < Composition < Chemsys < SG# ≪ Elements, where error bars correspond to $\sigma(\{\text{MAE}\}_K)$. Several key conclusions arise. For this particular dataset and model, using a single training model for inference (blue bars) generally produces an expected MAE ∼10–20% higher than using the ensemble of models from nested CV (green bars) across all C_K. From a different perspective, one would overestimate the expected MAEs by ∼10–20% if using the ensemble of non-nested K-fold models to perform inference for materials screening exercises, compared to the MAEs calculated by nested (K, L)-folds. Further assigning all binaries to the train set generally helps but has less of an impact than model ensembling.

More importantly, the choice of C_K has a very strong influence on the expected MAE. The goal of this and many other
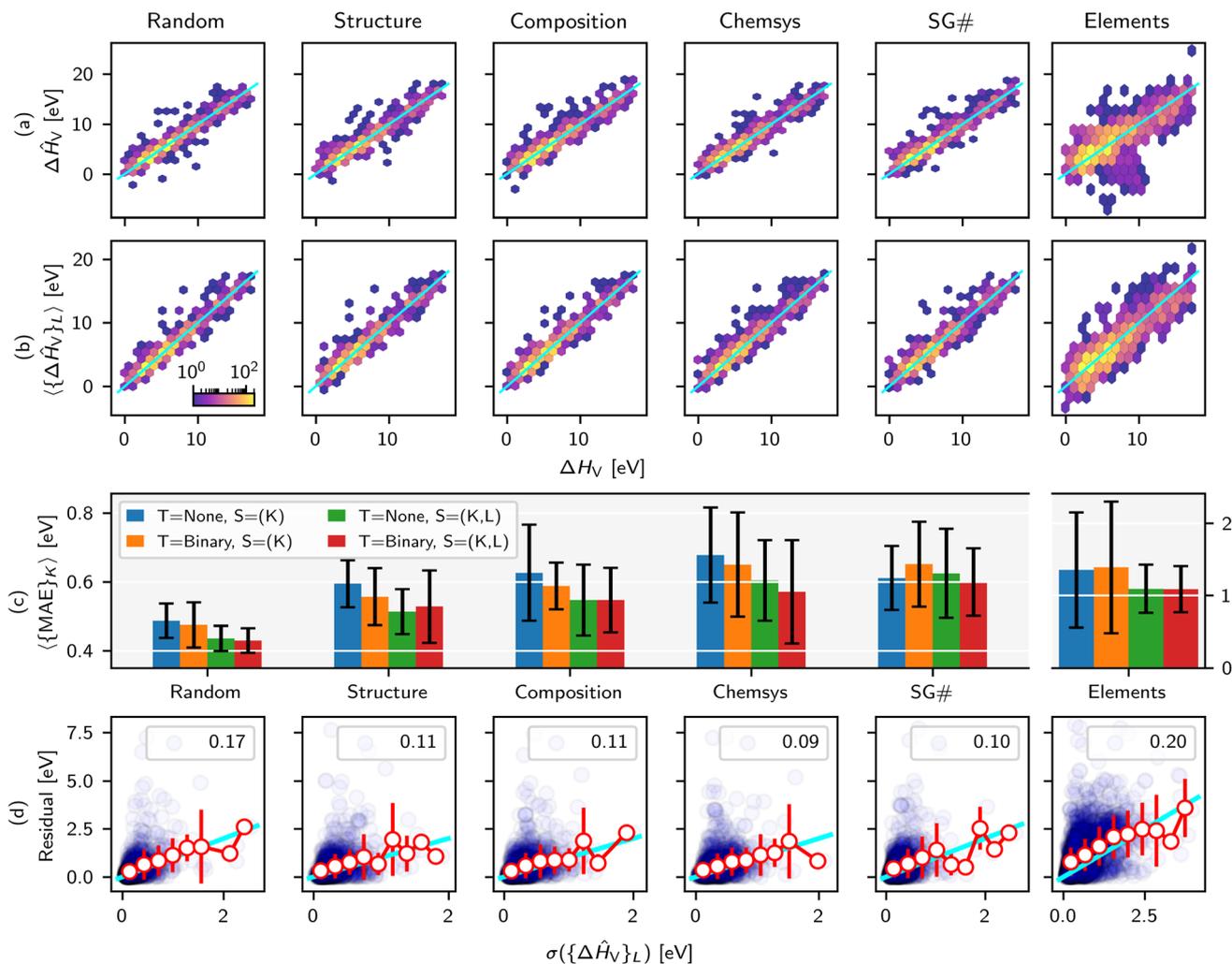
Fig. 2 ΔH_V test set parity plots for $D = 1.0$ and various C_K criteria for (a) $T =$ None and $S = (K)$ and (b) $T =$ Binary and $S = (K, L)$. (c) Expected MAE for various split criteria and combinations of other MatFold options such as $T = \{$None, Binary$\}$ and $S = \{K, (K, L)\}$. Quartile box plot of MAE and R^2 values are shown in ESI Fig. 5.† (d) Correlation of residual *vs.* standard deviation of ensemble predictions (purple circles), with R^2 shown in the inset. Additionally, within individual bins for $\sigma(\{\Delta \hat{H}_V\}_L)$, the average and standard deviation of residuals in that bin are shown with white circles and red error bars, respectively. The cyan line represents $y = x$.

specialty ML models for materials discovery, trained on small-to medium-sized datasets ($\sim$100s–1000s of examples), is to screen properties of structures that represent entirely new compositions, or even chemical systems, that are outside the training data. For this use case, performing a purely random split introduces substantial data leakage which leads to a $\sim$30% underestimation of the expected MAE when, for example, predicting defects in a structure that represents an unseen chemical system in the training data. As an even more extreme example, $C_K =$ Elements reveals a $\sim$2.5 times higher expected MAE than a purely random split, although ensembling can reduce expected MAE by $\sim$30% relative to a non-ensemble prediction.

Fig. 2d confirms that the standard deviation of predictions over model ensembles is a useful uncertainty metric[29,30] in this modeling application, but with some limitations. The individual residuals for any given test prediction (blue circles) are

only very weakly correlated with $\sigma(\{\Delta \hat{H}_V\}_L)$. However, computing the average and standard deviation of residuals within a given bin of $\sigma(\{\Delta \hat{H}_V\}_L)$ (red markers and error bars, respectively) collapses the data onto the $y = x$ parity line (cyan). Therefore, on average a low $\sigma(\{\Delta \hat{H}_V\}_L)$ is correlated with a low residual, but there is a non-negligible probability of individual predictions with very large residuals despite low uncertainty.

The final key insight from the MatFold analysis stems from the dependence of expected MAE on both C_K and D. Fig. 4 plots expected MAE for $D = \{0.1, 0.25, 0.5, 0.75, 1.0\}$, expressed on the x-axis in units of number of defect examples in the training data. Data leakage and underestimation of expected MAE are even more pronounced for the smallest dataset, and the rapid plateauing of the expected MAE with increasing data is potentially indicative of the absolute accuracy limit of the model. For more realistic screening criteria, *i.e.*, $C_K = \{$Composition, Structure, Chemsys$\}$, large accuracy gains are and will continue

to be obtained with increasing data collection. Interestingly (and perhaps intuitively), for C_K = Chemsys the improvement qualitatively appears to be saturating before the other criteria, but will only be confirmed with additional data collection. Finally, C_K = Elements reveals that additional data collection does not increase the accuracy during inference on compounds containing unseen elements. In fact, the error slightly increased intermittently with additional data collection because it may have introduced compounds with new test set elements which are even more difficult to extrapolate to from the elements contained in the train set (see ESI† for more details).

Surface work function exemplar

To gain insights into generalization error trends for a different type of dataset and ML model, we utilize MatFold on our dataset of 58 332 work functions, ϕ, of surfaces (generated from 3716 bulk crystals that have a zero band gap) calculated by density functional theory (DFT).[22] On average, each unique bulk crystal structure has ~15 derived surfaces. The dataset contains work functions of elemental (261), binary (14 623), and ternary (43 448) crystalline surfaces. The ML model trained on this dataset was based on a random forest (RF) model and a physics-motivated custom featurization of the top-most three atomic surface layers considering their electron affinities, atomic radii, ionization energy, Mendeleev number as well as structural information in the form of area packing fraction and interlayer spacing (details explained in our previous work[22]). The final RF model trained with 15 features has a test-MAE of 0.09 eV utilizing a random 90/10 split and 5-fold CV for hyperparameter optimization. This MAE is about 4–5 times better than the best benchmarking model and more than six times better than the random baseline. The model enabled the discovery of surfaces with extreme work functions for thermionic energy conversion[31] and high-brightness photocathodes.[32,33] Studying this dataset with MatFold is especially interesting as it significantly differs from the defect dataset in size, classes of materials, and model architecture.

We utilize similar split possibilities as for the defect dataset (see Table 2), except we do not automatically assign binary compounds to the training set (i.e., here we use only T = None). Moreover, for the LOO splits we excluded labels that make up less than 5% or more than 40% of the whole dataset to avoid unbalanced test set sizes (the user can specify these thresholds in MatFold). A total of 4046 unique splits were generated. As discussed in the previous section and Fig. 2 for the defect dataset, Fig. 3a and b show density parity plots of all outer test set (D = 1.0) predictions for C_K = {Random, Structure, Composition, Chemsys, SG#, Elements} for non-nested $S = K$-fold and nested $S = (K, L)$-fold, respectively.

Fig. 3c summarizes the MAEs for the parity plots displayed in (a) and (b). Unlike the defect dataset, the MAEs and their standard deviations for the work function dataset are very similar between the non-nested and nested splitting strategies. This likely stems from the GNN-based model being more prone to overfitting compared to the 15-feature RF model. Hence, the GNN model benefits more from statistical averaging during

nested splitting. Like the defect dataset, the MAEs increase in the order Random < Structure < Composition < Chemsys < Elements. However, an interesting difference is that the SG# split exhibits the highest MAE, less than the MAE for the Elements split (219 and 149 meV, respectively for nested splits). Compared to the MAE of the random split this is an increase of 133% and 59%, respectively. This agrees well with the RF model features being largely comprised of elemental properties (e.g., electron affinity) while containing little structural information. The work function model generalizes better outside the elemental training distribution and worse outside the structural training distribution. Among all splits that leave one element out, the MAEs are significantly larger for holding out F, H, O, or Cl (1178, 959, 708, 657 meV, respectively; cf. periodic table heat map in ESI Fig. 8†). These elements typically exhibit complex chemical behavior that may not be well captured in other chemistries. Compared to random splitting the MAE (94 meV) increases by only ~17% for structural, compositional, and chemical systems splitting (all three have an MAE of ~110 meV for nested splits). This surprisingly small increase in MAE may be explained by the work function strongly depending on the element present in the topmost surface layer – hence, as long as an element is present in any chemical system (or composition) in the train set, the RF model is able to learn the elemental trend for the work function and can then extrapolate well for an unseen chemical system. The average MAE increases (218 meV) by holding out groups of the periodic table compared to holding out just Elements (149 meV). Similarly, the MAEs increase by holding out point groups (227 meV) and crystal systems (272 meV) compared to just holding out space groups (219 meV). ESI Fig. 6† displays the parity plots, MAE trends, and residuals for these additional hold-out strategies.

Similar to Fig. 2d, the residuals $|\phi - \langle\{\hat{\phi}_L\}\rangle|$ are plotted against the standard deviation of the work function predictions over model ensembles in Fig. 3d. Interestingly, the averages of the residuals within a given bin of $\sigma(\{\hat{\phi}\}_L)$ (red markers) tend to have a slightly greater slope than the $x = y$ parity line (cyan). The overconfidence of this bootstrapped uncertainty metric appears to be typical of tree-based models using hand-engineered features and therefore requires re-calibration[3] such that the expectation value of the residual for a given σ bin is closer to parity.

Fig. 4b shows the dataset size dependence of the MAEs and their standard deviations for the work function dataset. A roughly linear decrease in the MAEs is observed with a logarithmic increase in the dataset size for splitting strategies C_K = {Random, Structure, Composition, and Chemsys}. The standard deviations of the MAEs typically decrease with increasing dataset size. However, for splitting strategies C_K = {SG#, Elements}, the MAEs start to plateau with increasing data size, indicating that additional data may no longer improve the RF model's capability to infer OOD samples accurately.

MatBench bulk modulus exemplar

The ΔH_V and ϕ exemplars (1) contain relatively small datasets in terms of unique structures, (2) represent local property
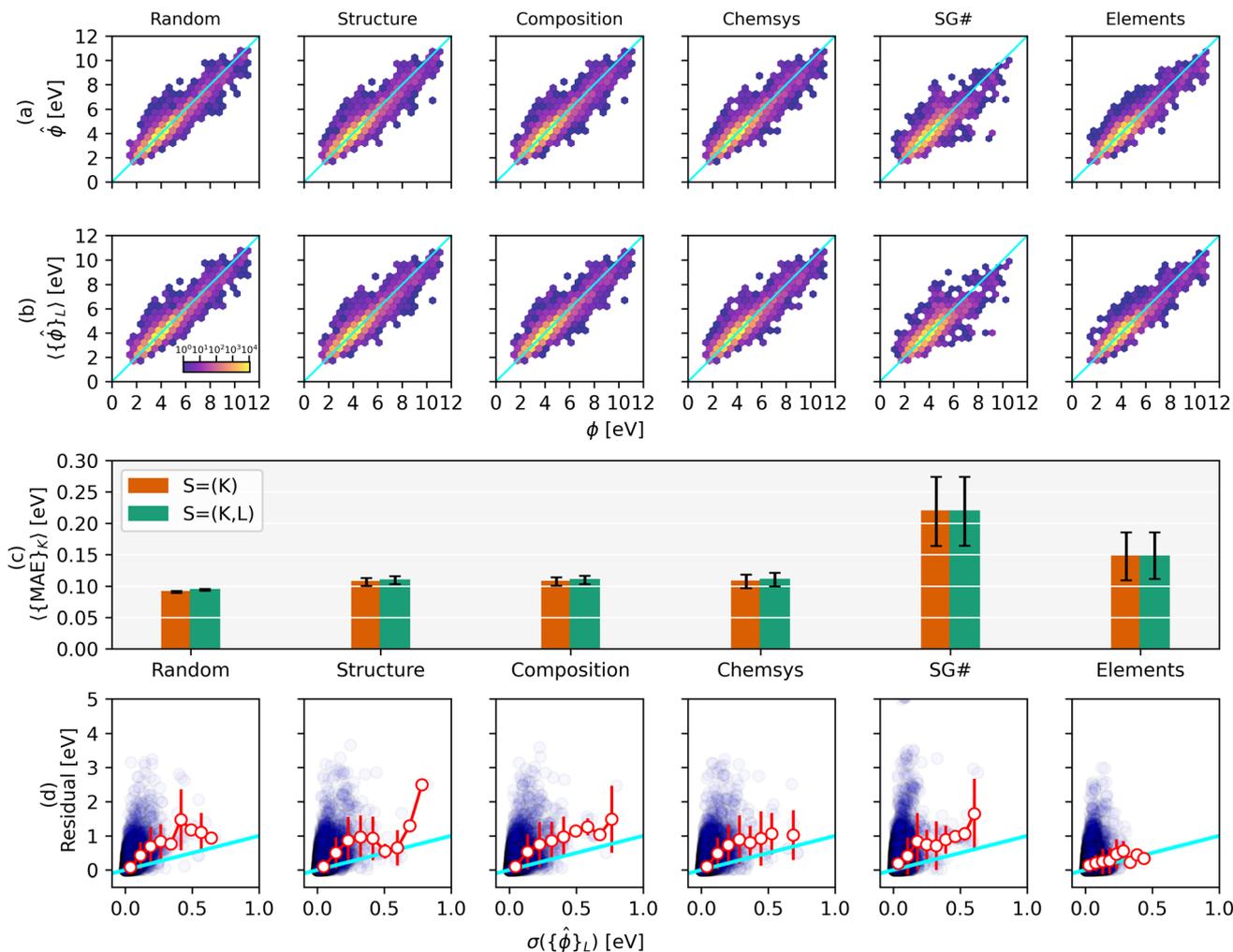
Fig. 3 Parity plots of DFT-calculated *vs.* ML-predicted work functions are shown for (a) K-fold and (b) nested (K, L)-fold splits for different splitting strategies. The color scale is on a logarithmic scale w.r.t. the number of structures at that grid point. The corresponding MAEs are displayed in (c) for K-fold and nested (K, L)-fold splits in green and orange, respectively. Quartile box plot of MAE and R^2 values are shown in ESI Fig. 7.† The residuals, $|\phi - \langle\{\hat{\phi}\}_L\rangle|$, are plotted *vs.* the standard deviation of the work function predictions (nested K-fold) in (d) alongside the average and standard deviation of residuals in 9 bins (white circles and red error bars, respectively). The individual residuals and corresponding standard deviations exhibit a negative R^2 value for all splitting strategies. All units are in eV and the $x = y$ line is highlighted in cyan.

prediction tasks (*i.e.*, multiple target values exist per unique structure), and (3) require specialty modeling approaches *via* the aforementioned GNN and RF works, respectively. Meanwhile, the Voigt–Reuss–Hill averaged bulk modulus, K_{VRH} MatBench[9] dataset represents a global property prediction task ($1 : 1$ mapping between $\approx 10\,000$ unique structures and their target property) that can be generally modeled by either structure-based models (*e.g.*, GNN) or compositionally-derived feature models (*e.g.*, RF). MatFold-automated CV can readily be applied to this standard benchmarking MatBench dataset, where data exists in larger quantities and contains materials with elements spanning nearly the entire periodic table.

Fig. 5 shows $(K = 5, L = 5)$-fold test set predictions for $C_K = \{\text{Structure}, \text{SG\#}, \text{Elements}\}$ and $(K = \text{LOO}, L = 5)$-fold test predictions for $C_K = \{\text{Elements}\}$. Fig. 5a and b show the difference in performance between a GNN approach (using a crystal graph convolutional neural network, CGCNN) and an RF

approach (using Magpie features), as detailed in MatBench.[9] Compared to the $C_K = \text{Structure}$ baseline, the GNN generalizes much better to unseen structural motifs ($C_K = \text{SG\#}$) than unseen elements ($C_K = \text{Elements}$) with a 9% *vs.* 41% increase, respectively, which is qualitatively consistent with observations in the ΔH_V exemplar. The RF model shows an even larger 18% MAE increase for $C_K = \text{SG\#}$ compared to its own $C_K = \text{Structure}$ baseline. For either modeling approach, the $C_K = \text{Elements}$ (LOO) have an $\langle\{\text{MAE}\}_K\rangle$ that is notably larger than the $C_K = \text{Structure}$ baseline, but the median test set error is comparable, driven by a very large skew for some elemental test sets that are very poorly predicted.

Fig. 5b demonstrates that inner nested ensembles of structure-based models (GNN) produce an uncertainty metric that is close to parity with the residual on average (*i.e.*, $\langle\text{Residual}|_\sigma\rangle \approx \sigma$). While for a composition-based model, this metric tends to be overconfident (*i.e.*, $\langle\text{Residual}|_\sigma\rangle > \sigma$).

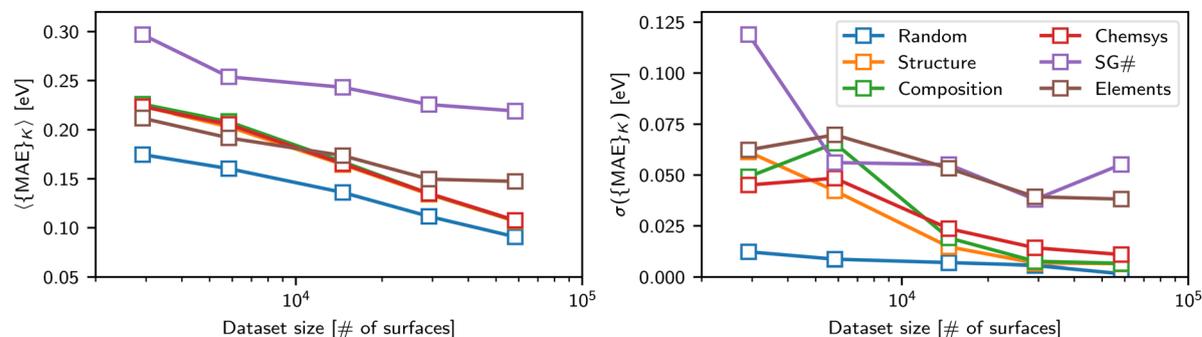(a) ΔH_V dataset
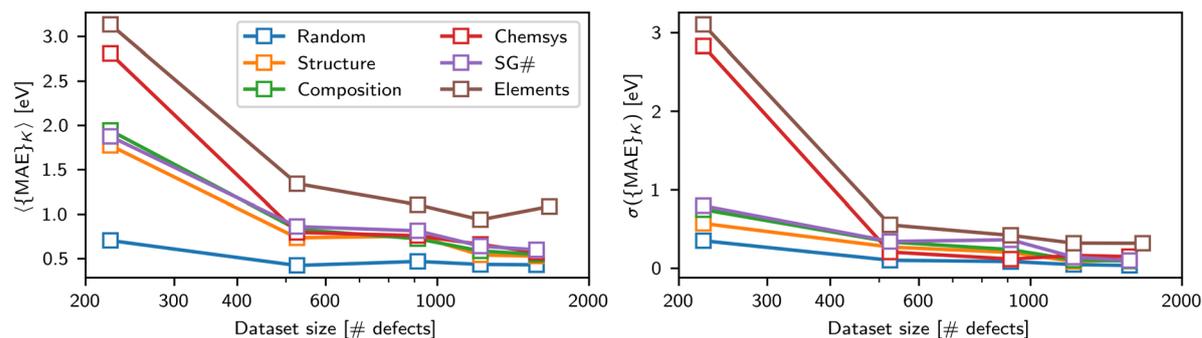
(b) Work function dataset

Fig. 4 The MAEs (left panels) and standard deviations of the MAEs (right panels) are plotted as a function of dataset size and splitting strategy for (a) the defect dataset and (b) the work function dataset.

Interestingly, this observation is consistent with the previous exemplars, despite the significant differences between all three ΔH_V, ϕ, and $\log(K_{VRH})$ datasets and modeling tasks. Nonetheless the uncertainty metric remains only very weakly correlated with the individual residuals (*cf.* R^2 values stated in the respective Figures).

Finally, Fig. 5c presents a parity plot of the residuals from C_K = {Element (LOO), SG#} *vs.* the residuals from C_K = Structure for each dataset and models corresponding to $D = 1.0$, $T =$ None, and $S = (K, L)$. Notably, there can be strong correlations ($R^2 > 0.7$) between them: many large prediction errors are simply because the structure itself is OOD with respect to all other structures in the dataset and does not specifically arise from being OOD with respect to the stricter splitting criteria. However, models/datasets with the lowest R^2 values arise because the test set residuals for C_K = Element (LOO) or C_K = SG# are much larger than the residuals for C_K = Structure. Here the stricter splitting criteria is enforcing the OOD test prediction, which otherwise is trivial because the structure is too similar to another in the dataset.

Discussion

MatFold provides an automated, easy-to-use tool for generating CV splits of materials data and ultimately enables deeper insights into a data-driven modeling approach's generalizability, uncertainty, and improvability. By computing expected error as a function of the splitting criteria in MatFold, one can both estimate OOD performance (*via* material featurization-agnostic CV splits) and readily and systematically decouple the expected generalization performance of a given modeling approach from its training dataset size. This can be combined with nested CV and bootstrapped model ensembles to ascertain the potential to mitigate over-fitting of high error outliers and the fidelity of uncertainty estimates. Finally, combining all of the above with fractional data hold-out indicates whether continued data collection is beneficial, and most importantly, how it depends on the OOD inference task probed by the different splitting criteria.

Some intuitive similarities and differences in MatFold CV trends can be observed between different modeling approaches and data domains, as demonstrated in our three exemplars. As expected in these exemplars, purely random splits provide the most biased underestimation of expected MAE, but the evolution of expected MAE with increasingly strict splitting criteria is heavily dependent on the modeling approach and data domain. For GNN's predictions of ΔH_V (a direct crystal structure input model), the expected MAE on structures with unseen elements is nearly double that of structures with unseen space groups. Yet the opposite is true for RF predictions of ϕ (a hand-engineered feature input model). Therefore these ΔH_V GNN models generalize better to unseen structural motifs than unseen chemistry, the exact opposite of the ϕ RF models. Trained on smaller datasets and even more sensitive to local structural features (*e.g.*, when a vacancy defect site itself corresponds to the held out element), these local property models'
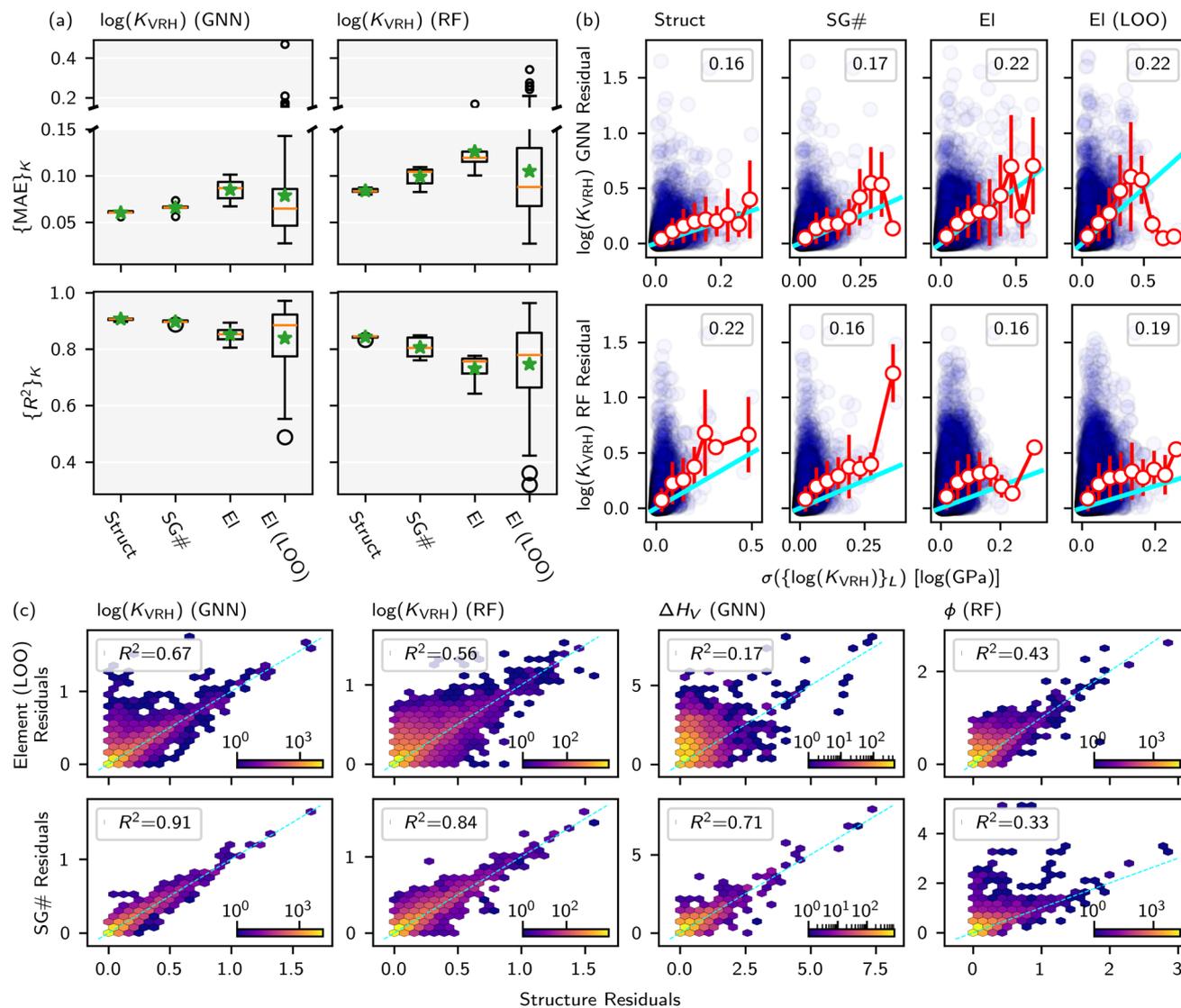
Fig. 5 (a) Quartile box plot of MAE and R^2 test set statistics for $\log(K_{VRH})$ using both RF-based and GNN-based models and various splitting criteria. Green stars represent the average over test sets. (b) For RF and GNN $\log(K_{VRH})$ models and different splitting criteria, correlation of residual *vs.* standard deviation of ensemble predictions (purple circles), with R^2 shown in the inset. Within individual bins for $\sigma(\{\log(\hat{K}_{VRH})\}_L)$, the average and standard deviation of residuals in that bin are shown with white circles and red error bars, respectively. The cyan line represents $y = x$. (c) The parity plot of residuals from C_K = {Element (LOO), SG#} *vs.* the residuals from C_K = Structure for each dataset and model corresponding to $D = 1.0$, $T = $ None, and $S = (K, L)$. Color bars indicate logarithmically the number of test predictions in a given bin.

expected error showed higher sensitivity to the splitting criteria than a global property model trained on a much larger dataset (the MatBench bulk modulus). This further highlights the need for performing the comprehensive and automated CV splitting analysis enabled by MatFold in any given study to gain a detailed and unbiased perspective on a materials discovery model's generalization limitations.

The ΔH_V GNN predictions also benefit substantially from bootstrapped model ensembling to reduce over-fitting and mitigate outliers in test set prediction parity, while no benefit is observed in the ϕ RF models. Consequently, we observed the need to re-calibrate the bootstrapped uncertainty metric derived for the ϕ RF models, but not for the ΔH_V GNN models. This observation also holds true for both GNN *vs.* RF models trained

for the same global property $\log(K_{VRH})$ modeling task. It should be noted that re-tuning the hyperparameters during model ensembling could further reduce over-fitting but comes at a large computational cost (*e.g.*, tuning 2 hyperparameters with 10 possible values each would already require training 100 times more models). Finally, in both ΔH_V and ϕ exemplars, we generally observe continued improvement in model performance with more training data for moderately difficult OOD inference (*e.g.*, structure, composition, or chemsys splits). However, for their weakest inference task (Elements for ΔH_V GNN and SG# for ϕ RF models), neither is likely to improve further with additional data indicating fundamental limitations of the respective model architectures.

We anticipate that the splitting criteria and other functionality introduced by MatFold will lower the bar for better and more automated CV of data-driven materials models. Practitioners will have a better understanding of their expected accuracy for materials discovery in increasingly difficult OOD inference, regardless of their modeling approach because MatFold CV splits are only material dependent and entirely material featurization-agnostic. This will also enable deeper insights of materials discovery performance spanning differing modeling approaches and data domains and, if widely adopted, provide more grounded evidence for which modeling approaches may be more appropriate in various materials discovery situations.

Code availability

The code is available open-source on GitHub (at **https://github.com/d2r2group/MatFold**) and can be installed by pip. A frozen version of the code is permanently accessible on Zenodo *via* this link: **https://doi.org/10.5281/zenodo.13147391**.

Data availability

The work function database is available for download at **https://doi.org/10.5281/zenodo.10381505**. The ΔH_V data,[21,28] is available for download from its original source at **https://doi.org/10.5281/zenodo.8087871**[27] and **https://doi.org/10.1021/jacs.1c05570**. We summarize the data in supplementary_files_defects.zip file that contains all CIF files and a CSV file with the corresponding structure name, index of the vacancy defect, and vacancy formation energy.

Author contributions

M. D. W. performed writing – original draft (lead); review and editing (equal); software (equal); methodology (equal); visualization (lead); investigation (equal); data curation (equal); conceptualization (lead); supervision (equal); resources (equal). P. S. performed writing – original draft (supporting); review and editing (equal); software (equal); methodology (equal); visualization (supporting); investigation (equal); data curation (equal); conceptualization (supporting); supervision (equal); resources (equal).

Conflicts of interest

There are no conflicts of interest to declare.

Acknowledgements

References

1 D. Morgan and R. Jacobs, Opportunities and Challenges for Machine Learning in Materials Science, *Annu. Rev. Mater. Res.*, 2020, **50**, 71–103.

2 R. Jacobs, L. E. Schultz, A. Scourtas, K. J. Schmidt, O. Price-Skelly, W. Engler, I. Foster, B. Blaiszik, P. M. Voyles and D. Morgan, Machine Learning Materials Properties with Accurate Predictions, Uncertainty Estimates, Domain Guidance, and Persistent Online Accessibility, *arXiv*, 2024, preprint, DOI: **10.48550/arXiv.2406.15650**.

3 G. Palmer, S. Du, A. Politowicz, J. P. Emory, X. Yang, A. Gautam, G. Gupta, Z. Li, R. Jacobs and D. Morgan, Calibration after bootstrap for accurate uncertainty quantification in regression models, *npj Comput. Mater.*, 2022, **8**, 115.

4 S. Jiang, S. Qin, R. C. Van Lehn, P. Balaprakash and V. M. Zavala, Uncertainty quantification for molecular property predictions with graph neural architecture search, *Digital Discovery*, 2024, **3**(8), 1534–1553, DOI: **10.1039/D4DD00088A**.

5 J. Gawlikowski, C. R. N. Tassi, M. Ali, J. Lee, M. Humt, J. Feng, A. Kruspe, R. Triebel, P. Jung, R. Roscher, M. Shahzad, W. Yang, R. Bamler and X. X. Zhu, A survey of uncertainty in deep neural networks, *Artif. Intell. Rev.*, 2023, **56**, 1513–1589.

6 D. Baumann and K. Baumann, Reliable estimation of prediction errors for QSAR models under model uncertainty using double cross-validation, *J. Cheminf.*, 2014, **6**, 1–19.

7 S. K. Kauwe, J. Graser, R. Murdock and T. D. Sparks, Can machine learning find extraordinary materials?, *Comput. Mater. Sci.*, 2020, **174**, 109498.

8 B. Meredig, E. Antono, C. Church, M. Hutchinson, J. Ling, S. Paradiso, B. Blaiszik, I. Foster, B. Gibbons, J. Hattrick-Simpers, A. Mehta and L. Ward, Can machine learning identify the next high-temperature superconductor?

Examining extrapolation performance for materials discovery, *Mol. Syst. Des. Eng.*, 2018, **3**, 819–825.

9 A. Dunn, Q. Wang, A. Ganose, D. Dopp and A. Jain, Benchmarking materials property prediction methods: the Matbench test set and Automatminer reference algorithm, *npj Comput. Mater.*, 2020, **6**, 138.

10 S. S. Omee, N. Fu, R. Dong, M. Hu and J. Hu, Structure-based out-of-distribution (OOD) materials property prediction: a benchmark study, *npj Comput. Mater.*, 2024, **10**, 144.

11 J. Hu, D. Liu, N. Fu and R. Dong, Realistic material property prediction using domain adaptation based machine learning, *Digital Discovery*, 2024, **3**, 300–312.

12 K. Li, B. DeCost, K. Choudhary, M. Greenwood and J. Hattrick-Simpers, A critical examination of robustness and generalizability of machine learning prediction of materials properties, *npj Comput. Mater.*, 2023, **9**, 1–9.

13 H. Zhang, W. Chen, J. M. Rondinelli and W. Chen, *ET-AL*, Entropy-targeted active learning for bias mitigation in, *Appl. Phys. Rev.*, 2023, **10**(2), 021403.

14 Z. Wu, B. Ramsundar, E. N. Feinberg, J. Gomes, C. Geniesse, A. S. Pappu, K. Leswing and V. Pande, MoleculeNet: a benchmark for molecular machine learning, *Chem. Sci.*, 2018, **9**, 513–530.

15 Z. Xiong, Y. Cui, Z. Liu, Y. Zhao, M. Hu and J. Hu, Evaluating explorative prediction power of machine learning algorithms for materials discovery using k-fold forward cross-validation, *Comput. Mater. Sci.*, 2020, **171**, 109203.

16 R. P. Sheridan, Time-Split Cross-Validation as a Method for Estimating the Goodness of Prospective Prediction, *J. Chem. Inf. Model.*, 2013, **53**, 783–790.

17 K. Li, D. Persaud, K. Choudhary, B. DeCost, M. Greenwood and J. Hattrick-Simpers, Exploiting redundancy in large materials datasets for efficient machine learning with less data, *Nat. Commun.*, 2023, **14**, 1–10.

18 K. Li, A. N. Rubungo, X. Lei, D. Persaud, K. Choudhary, B. DeCost, A. B. Dieng and J. Hattrick-Simpers, Probing out-of-distribution generalization in machine learning for materials, *arXiv*, 2024, preprint, arxiv:2406.06489, DOI: **10.48550/arXiv.2406.06489**.

19 T. Xie and J. C. Grossman, Crystal Graph Convolutional Neural Networks for an Accurate and Interpretable Prediction of Material Properties, *Phys. Rev. Lett.*, 2018, **120**, 145301.

20 L. Ward, A. Agrawal, A. Choudhary and C. Wolverton, A general-purpose machine learning framework for predicting properties of inorganic materials, *npj Comput. Mater.*, 2016, **2**, 16028.

21 M. D. Witman, A. Goyal, T. Ogitsu, A. H. McDaniel and S. Lany, Defect graph neural networks for materials discovery in high-temperature clean-energy applications, *Nat. Comput. Sci.*, 2023, **3**, 675–686.

22 P. Schindler, E. R. Antoniuk, G. Cheon, Y. Zhu and E. J. Reed, Discovery of Stable Surfaces with Extreme Work Functions by High-Throughput Density Functional Theory and Machine Learning, *Adv. Funct. Mater.*, 2024, **2401764**, 1–12.

23 C. Chen, W. Ye, Y. Zuo, C. Zheng and S. P. Ong, Graph Networks as a Universal Machine Learning Framework for Molecules and Crystals, *Chem. Mater.*, 2019, **31**, 3564–3572.

24 K. Choudhary, B. DeCost, L. Major, K. Butler, J. Thiyagalingam and F. Tavazza, Unified graph neural network force-field for the periodic table: solid state applications, *Digital Discovery*, 2023, **2**, 346–355.

25 B. Deng, P. Zhong, K. Jun, J. Riebesell, K. Han, C. J. Bartel and G. Ceder, CHGNet as a pretrained universal neural network potential for charge-informed atomistic modelling, *Nat. Mach. Intell.*, 2023, **5**, 1031–1041.

26 I. Batatia, *et al.*, A foundation model for atomistic materials chemistry, *arXiv*, 2023, preprint, arXiv:2401.00096, DOI: **10.48550/arXiv.2401.00096**.

27 M. Witman, A. Goyal, T. Ogitsu, A. H. McDaniel and S. Lany, *A database of vacancy formation enthalpies for materials discovery (0.0.1) [dataset]*, Zenodo, 2023, DOI: **10.5281/zenodo.8087871**.

28 R. B. Wexler, G. S. Gautam, E. B. Stechel and E. A. Carter, Factors Governing Oxygen Vacancy Formation in Oxide Perovskites, *J. Am. Chem. Soc.*, 2021, **143**, 13212–13227.

29 H.-J. Lu, N. Zou, R. Jacobs, B. Afflerbach, X.-G. Lu and D. Morgan, Error assessment and optimal cross-validation approaches in machine learning applied to impurity diffusion, *Comput. Mater. Sci.*, 2019, **169**, 109075.

30 V. Agrawal, S. Zhang, L. E. Schultz and D. Morgan, Accelerating Ensemble Error Bar Prediction with Single Models Fits, *arXiv*, 2024, preprint, arxiv:2404.09896, DOI: **10.48550/arXiv.2404.09896**.

31 P. Schindler, D. C. Riley, I. Bargatin, K. Sahasrabuddhe, J. W. Schwede, S. Sun, P. Pianetta, Z.-X. Shen, R. T. Howe and N. A. Melosh, Surface Photovoltage-Induced Ultralow Work Function Material for Thermionic Energy Converters, *ACS Energy Lett.*, 2019, **4**, 2436–2443.

32 E. R. Antoniuk, P. Schindler, W. A. Schroeder, B. Dunham, P. Pianetta, T. Vecchione and E. J. Reed, Novel Ultrabright and Air-Stable Photocathodes Discovered from Machine Learning and Density Functional Theory Driven Screening, *Adv. Mater.*, 2021, **33**, 2104081.

33 E. R. Antoniuk, Y. Yue, Y. Zhou, P. Schindler, W. A. Schroeder, B. Dunham, P. Pianetta, T. Vecchione and E. J. Reed, Generalizable density functional theory based photoemission model for the accelerated development of photocathodes and other photoemissive devices, *Phys. Rev. B*, 2020, **101**, 235447.